

ELECTROMAGNETIC FORM FACTORS OF THE NUCLEON

HARTMUT SCHMIEDEN

Physikalisches Institut

Nussallee 12

D-53115 Bonn, Germany

E-mail: schmieden@physik.uni-bonn.de

Elastic form factors provide information about the low energy structure of composite particles. Recent double polarization coincidence experiments significantly improved our knowledge of proton and neutron form factors. Recoil polarization measurements in the $p(\vec{e}, e' \vec{p})$ reaction proved that at momentum transfers above $Q^2 \simeq 1.5 (\text{GeV}/c)^2$ the electric form factor of the proton falls significantly faster than the dipole expectation. The close-to-dipole shape at low Q^2 of the neutron magnetic form factor is now confirmed by independent measurements. For the neutron electric form factor ${}^3\vec{H}e(\vec{e}, e' n)$, $\vec{D}(\vec{e}, e' n)$ and $D(\vec{e}, e' \vec{n})$ double polarization experiments have provided model independent results, within their statistical errors in agreement with the Galster parameterization.

1. Introduction

In today's view the nucleon is composed of pointlike, almost massless current quarks and gluons as the mediators of the color forces between them. The dynamics is described by the quantum field theory of strong interaction, QCD. It is well tested at very high energies and momentum transfers, where the mutual interaction is weak enough for perturbative methods to be applicable. The nucleon appears dramatically different at low energies (where we find our surrounding matter). Here the non-linearity of QCD prohibits any exact *ab initio* calculation of hadron properties. This is the regime of constituent quarks as effective, multi-body degrees of freedom and the light mesons as the Goldstone bosons of chiral symmetry breaking. As for any composite, non-pointlike quantum mechanic particle ¹ a whole excitation spectrum builds upon the nucleon ground state. Although there remain decisive problems concerning the total number and individual nature of states, the basic properties of the spectrum can be successfully reproduced by constituent quark models ². However, the transition between

the current and constituent quark regimes is not understood. Lattice QCD and chiral extrapolations yield hints for the masses of effective constituents³, but dynamically generated constituent quarks could not yet been identified⁴. Nevertheless, first promising results have been obtained for ground state properties like magnetic moments, polarizabilities and form factors⁵.

The intimate connection of ground state observables to the high energy structure is made explicit by the concept of generalized parton distributions $H, \tilde{H}, E, \tilde{E}$ in exclusive deep inelastic reactions⁶. At vanishing (Mandelstam) $t \rightarrow 0$ they fade to the usual unpolarized and polarized parton distributions for quarks and antiquarks⁷,

$$H \rightarrow q(x) \quad \tilde{H} \rightarrow \Delta q(x), \quad (1)$$

whereas in the non-perturbative regime of small but finite t integration over Björken x yields the Dirac, Pauli and axial form factors⁸,

$$\int_{-1}^1 dx H = F_1(t) \quad \int_{-1}^1 dx E = F_2(t) \quad (2)$$

$$\int_{-1}^1 dx \tilde{H} = g_A(t) \quad \int_{-1}^1 dx \tilde{E} = h_A(t). \quad (3)$$

The elastic form factors parameterize the ability of the composite nucleon to incorporate a momentum transfer, \vec{q} , coherently, i.e. without excitation and particle emission. They are related to the distribution of charge and currents and therefore of fundamental importance for the understanding of nucleon structure.

Lepton scattering is a unique tool for the investigation of the electromagnetic structure of the nucleon. In the simplest approximation, it is characterized by the exchange of one virtual photon, which transfers the momentum \vec{q} and the energy ω . Electron scattering covers the spacelike region, because the squared four-momentum transfer, $q^2 = \omega^2 - \vec{q}^2$, is always negative. It is therefore usually expressed by the positive quantity $Q^2 = -q^2 > 0$. The timelike region, where $Q^2 < 0$, can be accessed through electron-positron annihilation into a pair of proton and anti-proton⁹ or neutron and anti-neutron¹⁰.

In elastic electron-nucleon scattering the charge-current density of the nucleon can be written in the form¹¹:

$$\bar{N}\Gamma_\mu N = \bar{N} \left[\gamma_\mu F_1(Q^2) + \frac{i\sigma_{\mu\nu}q^\nu}{2m_N} \kappa F_2(Q^2) \right] N. \quad (4)$$

The *Dirac* form factor, $F_1(Q^2)$, modifies the vector current of charge and normal magnetic moment, whereas the *Pauli* form factor, $F_2(Q^2)$, param-

eterizes the effect of the anomalous magnetic moment, κ , as motivated by the Gordon decomposition of the electromagnetic current. Linear combinations of F_1 and F_2 constitute the electric and magnetic *Sachs* form factors¹²

$$G_E^{n,p}(Q^2) = F_1^{n,p}(Q^2) - \tau \kappa_{n,p} F_2^{n,p}(Q^2) \quad (5)$$

$$G_M^{n,p}(Q^2) = F_1^{n,p}(Q^2) + \kappa_{n,p} F_2^{n,p}(Q^2), \quad (6)$$

where $\tau = Q^2/4m_N^2$ is a dimensionless measure of the squared four-momentum transfer in units of the nucleon rest mass, m_N . At $Q^2 \rightarrow 0$ these form factors correspond to the total charge and magnetic moment of protons and neutrons:

$$G_E^{n,p}(Q^2 \rightarrow 0) = 0, 1 \quad (7)$$

$$G_M^{n,p}(Q^2 \rightarrow 0) = -1.91, 2.79. \quad (8)$$

In the particular reference frame with vanishing energy transfer, the *Breit* frame, G_E and G_M have been interpreted as the Fourier transforms of the corresponding distributions of charge and magnetism¹². Recently, the possibility of interpretation of G_E in terms of the intrinsic charge distribution was controversially discussed again^{13,14,15,16}.

With the Sachs form factors the cross section for elastic electron-nucleon scattering can be written in the famous *Rosenbluth* form,

$$\frac{d\sigma}{d\Omega} = \left(\frac{d\sigma}{d\Omega} \right)_{\text{Mott}} \cdot \left(\frac{G_E^2 + \tau G_M^2}{1 + \tau} + 2\tau G_M^2 \tan^2 \frac{\vartheta_e}{2} \right), \quad (9)$$

where $(d\sigma/d\Omega)_{\text{Mott}}$ is the Mott cross section for electron scattering off a pointlike spin- $\frac{1}{2}$ object and ϑ_e denotes the electron scattering angle. Due to their different angular weights in Eq.9, G_E and G_M can be experimentally separated at constant Q^2 .

The measurement of all Sachs form factors of proton and neutron enables the decomposition into isoscalar and isovector parts, important for the comparison to model calculations. Furthermore, using isospin invariance it is possible to extract u/d flavour specific form factors from $G_{E,M}^p$ and $G_{E,M}^n$. The extension to the electric and magnetic strange quark contributions requires additional observables. From parity violating elastic electron scattering the cross section asymmetry with regard to the helicity $+/-$ flip of the electron beam

$$A_{PV} = \frac{\sigma^+ - \sigma^-}{\sigma^+ + \sigma^-} \quad (10)$$

is extracted, which is due to the interference of γ and Z^0 exchange. It determines the Z form factors

$$G_{E,M}^Z = G_{E,M}^p - G_{E,M}^n - 4 \sin^2 \Theta_W G_{E,M}^p - G_{E,M}^s, \quad (11)$$

from which the strange form factors $G_{E,M}^s$ can be extracted, provided the Weinberg mixing angle, Θ_W , and the nucleon form factors $G_{E,M}^p$ and $G_{E,M}^n$ are sufficiently well known.

This talk reviews the current experimental status of the electromagnetic elastic nucleon form factors. Recent results concerning the proton electric form factor at high Q^2 are summarized in the next section. The neutron form factors are discussed in section 3. Measurements of G_M^n are addressed in subsection 3.1. Special emphasis is given to recent measurements of the neutron electric form factor using double polarization techniques in section 3.2. The paper concludes with a summary and outlook.

2. Proton form factors

The method of Rosenbluth-separation has been used in elastic electron-proton scattering^{17,18} to determine G_E^p and G_M^p up to $Q^2 \simeq 9 (\text{GeV}/c)^2$. At higher Q^2 up to $30 (\text{GeV}/c)^2$, G_M^p dominates the cross section and has thus been determined directly¹⁹. The result was that both G_M^p and G_E^p approximately follow the so-called dipole form and scale with the magnetic moment, μ_p :

$$G_E^p \simeq G_D = \left(1 + \frac{Q^2}{0.71 (\text{GeV}/c)^2}\right)^{-2}, \quad (12)$$

$$G_M^p \simeq \mu_p G_D. \quad (13)$$

However, due to the insensitivity of the cross section to G_E at higher Q^2 , the Rosenbluth separation yields large uncertainties for this quantity. Much improved sensitivity is obtained using double polarization observables in electron-nucleon scattering^{20,21}. The components of the recoil polarization in the $N(\vec{e}, e' \vec{N})$ reaction read

$$P_x = -P_e \frac{\sqrt{2\tau\epsilon(1-\epsilon)} G_E^N G_M^N}{\epsilon(G_E^N)^2 + \tau(G_M^N)^2} \quad (14)$$

$$P_y = 0 \quad (15)$$

$$P_z = P_e \frac{\tau\sqrt{1-\epsilon^2}(G_M^N)^2}{\epsilon(G_E^N)^2 + \tau(G_M^N)^2}, \quad (16)$$

where \hat{x} is in the electron scattering plane perpendicular to the direction of the momentum transfer, \hat{y} is normal to the scattering plane, and \hat{z} points

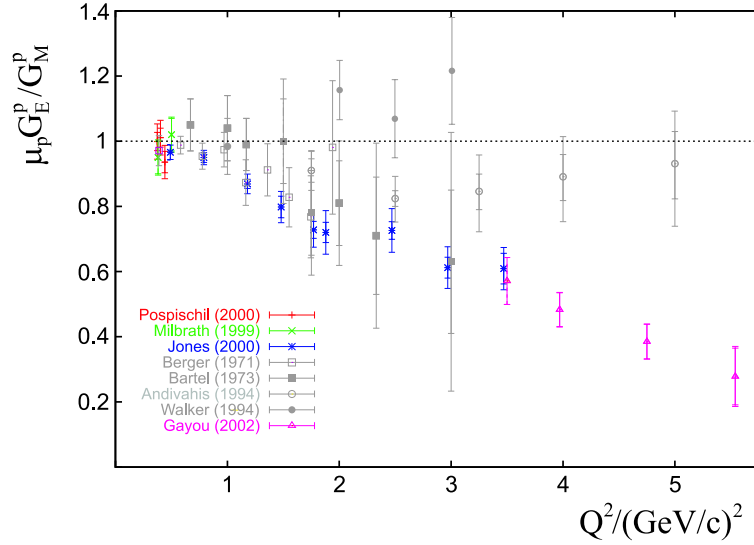


Figure 1. Results for $\mu_p G_E^p / G_M^p$ from unpolarized Rosenbluth^{29,30,31,32} and recoil polarization measurements^{23,24,25,27,28}.

into the direction of the momentum transfer, \vec{q} ; $\epsilon = (1 + \frac{2|\vec{q}|^2}{Q^2} \tan^2 \frac{\vartheta_z}{2})^{-1}$ is the photon polarization parameter and P_e denotes the longitudinal polarization of the electron beam. In particular, P_x is linear in G_E and the polarization ratio P_x/P_z is directly related to G_E/G_M .

The measurements of the Hall A collaboration at Jefferson Laboratory using a recoil polarimeter in one of the high resolution spectrometers²² show with high statistical precision a linear decrease of G_E^p/G_M^p up to $Q^2 = 5.6 (\text{GeV}/c)^2$ ^{23,24,25} (c.f. Fig. 1). The results have been included in new empirical form factor fits²⁶. At low Q^2 recoil polarization measurements^{27,28} are in agreement with form factor scaling, i.e. $\mu_p G_E^p / G_M^p = 1$.

3. Neutron form factors

Generally, the measurement of the neutron form factors raises more difficulties, because there is no free neutron target available which is suited for electron scattering experiments. The best possible approximation of free electron-neutron scattering is quasi-free scattering off the lightest nuclei. In $D(e, e')$ single arm experiments the dominating proton contribution has to be subtracted, with corresponding large uncertainties³³. A Rosenbluth-separation has nevertheless been achieved³⁴ up to $Q^2 = 4 (\text{GeV}/c)^2$. At

low Q^2 nuclear effects and final state interaction are well enough under control³⁵ to permit an extraction of G_M^n from inclusive quasi-elastic ${}^3\text{He}(\vec{e}, e')$ scattering with polarized beam and polarized target^{36,37,38}. $D(e, e'n)$ coincidence experiments allow the explicit tagging of electron-neutron scattering^{30,40,41,42,43,44}. The influence of binding effects can be minimized through the simultaneous measurement of the $D(e, e'p)$ reaction. Similar to G_M^p , the neutron magnetic form factor also roughly exhibits the dipole behaviour,

$$G_M^n \simeq \mu_n G_D. \quad (17)$$

The situation concerning the neutron electric form factor, G_E^n , is most unfavourable. It must vanish in the static limit, $G_E^n(Q^2 \rightarrow 0) = 0$, due to the zero charge of the neutron. The smallness of $(G_E^n)^2$ compared to $\tau(G_M^n)^2$ makes a Rosenbluth decomposition according to Eq.9 very difficult. Due to the corresponding large errors in the small quantity the extracted values for G_E^n are compatible with zero^{30,34}. Therefore, in the momentum transfer range $Q^2 < 1 (\text{GeV}/c)^2$ the most precise data came from *elastic* electron-deuteron scattering^{45,46}, where the structure function $A(Q^2)$ depends on the isoscalar form factor $(G_E^p + G_E^n)^2$ and thus provides a higher sensitivity to G_E^n through its interference with the large G_E^p . However, the necessary unfolding of the deuteron wavefunction introduces a substantial model dependence in the extracted neutron electric form factor. Reduced model dependence has been obtained analyzing the $e-d$ elastic quadrupole form factor⁴⁷. The model dependence can be overcome by exclusive $(e, e'n)$ double polarization experiments with polarized beam and either polarized target or recoil polarimetry.

3.1. Recent G_M^n experiments

Precise determinations of G_M^n come from unpolarized coincidence experiments at Bates⁴⁰, NIKHEF⁴¹, ELSA⁴², and MAMI^{43,44}. Except the Bates experiment, which measured the absolute $D(e, e'n)$ cross section, these experiments determined G_M^n from the ratio $R = \frac{\sigma(e, e'n)}{\sigma(e, e'p)}$ of quasi-free neutron over proton cross sections off the deuteron with simultaneous neutron/proton detection in one single hadron detector. In this ratio nuclear binding effects cancel to a large extent. Moreover, this method is also experimentally insensitive to luminosity fluctuations and detector acceptancies.

Nevertheless, detailed control of the hadron detectors absolute detection efficiency for protons and, particularly, neutrons is essential. The setups of

the various experiments have been very similar, with the electrons detected in a magnetic spectrometer and coincident n/p-detection in a well shielded plastic or mineral oil scintillator telescope. However, different approaches have been used to determine the absolute neutron detection efficiency. For the Bates and ELSA measurements "in situ" methods were chosen with a bremsstrahlung radiator positioned in front of the experimental target in order to exploit the $D(\gamma, p)n$ or $p(\gamma, \pi^+)n$ reactions, respectively, to tag neutrons in the telescope. In contrast, the hadron detectors which were used at MAMI and NIKHEF were calibrated at the PSI neutron beam in a kinematically complete $p(n, p)n$ experiment. This method relies on the good control and portability of the effective detector thresholds.

Figure 2 shows a comparison of the recent results from Bates ^{36,37,40}, ELSA ⁴², JLab ^{38,39}, NIKHEF ⁴¹, and MAMI ^{43,44}. Despite the individual errors of down to 2 %, the MAMI data are approximately 10 - 15 % below the ELSA ones. The probable origin of this discrepancy is the absolute neutron detection efficiency calibration. In this respect, the possible impact of untagged electroproduction events has been discussed for the in situ method ^{48,49}.

The measurement of the transverse asymmetry A_T from inclusive quasi-elastic ${}^3\text{He}(\vec{e}, e')$ scattering provides an alternative method for the extraction of G_M^n , which is completely independent of efficiency calibrations ^{36,37,38}. However, full Fadeev calculations are required with inclusion of final state interaction and meson exchange currents. Those are currently available for $Q^2 = 0.1$ and $0.2 (\text{GeV}/c)^2$ ^{35,38}, the results of a PWIA analysis for Q^2 up to $0.6 (\text{GeV}/c)^2$ ³⁹. The extracted values of G_M^n agree with the unpolarized measurements of Anklin et al. ^{41,43} and Kubon et al. ⁴⁴.

3.2. G_E^n double polarization experiments

Double polarization observables in exclusive quasi-free electron-deuteron scattering with longitudinally polarized electrons offer high sensitivity to G_E^n , due to an interference with the large G_M^n , combined with negligible dependence on the deuteron wavefunction ⁵⁰, e.g. in the recoil polarization observables of Eqs. 14 and 16. In the completely equivalent scattering $\vec{n}(\vec{e}, e'n)$ of longitudinally polarized electrons off a polarized neutron target the cross section asymmetry with regard to reversal of the electron beam polarization is given by

$$A = -P_e \frac{\sqrt{2\tau\epsilon(1-\epsilon)}G_E^n G_M^n \cdot \tilde{P}_x + \tau\sqrt{1-\epsilon^2}(G_M^n)^2 \cdot \tilde{P}_z}{\epsilon(G_E^n)^2 + \tau(G_M^n)^2}, \quad (18)$$

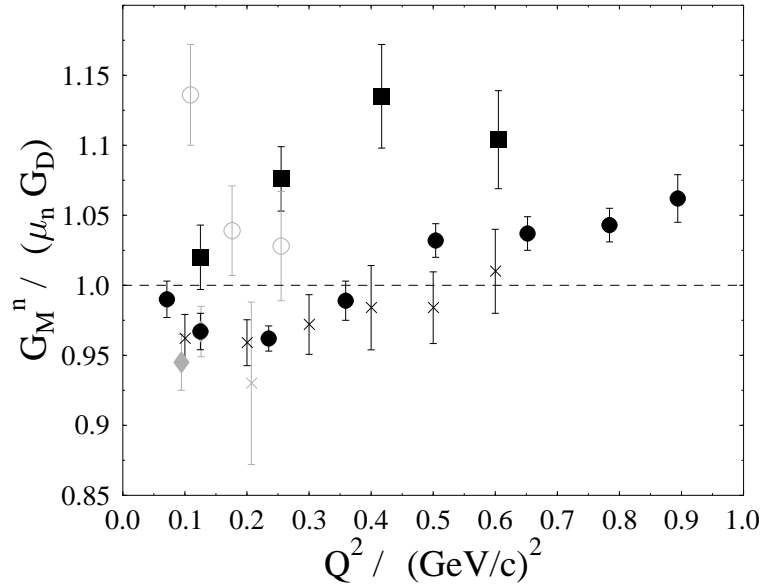


Figure 2. Results of recent G_M^n experiments. Gao et al.^{36,37} (grey cross) and Xu et al.^{38,39} (black crosses) exploited the $^3\text{He}(\vec{e}, e')$ cross section asymmetry. The open circles are the result of the $\text{D}(e, e'n)$ experiment of Markowitz et al.⁴⁰. The ELSA⁴² (full squares), NIKHEF⁴¹ (grey diamonds) and MAMI^{43,44} (full circles) measurements made use of the ratio method as described in the text.

where now $\vec{P}_{x,z}$ are the components of the initial state neutron polarization. The polarized target neutrons can be provided by polarized ^3He ^{51,52,53}, where the neutron carries approximately 87% of the polarization of the nucleus⁵⁴, or by vector polarized ^2D ^{55,56}. The measurement of asymmetry ratios yields independence of the absolute degree of the target polarization^{57,55}.

3.2.1. Polarized target experiments

First experiments aimed at the extraction of G_E^n from the inclusive quasi-elastic reaction $^3\text{He}(\vec{e}, e')$. The feasibility of such kind of experiments was successfully demonstrated, but the statistical accuracy remained unsatisfactory.

The magnetic moment of ^3He within 10% agrees with the free neutron one. Therefore the proton contribution in the measured asymmetries first was expected to be small⁵⁴. Later calculations, however, showed that

the remaining impact of the protons on the measured asymmetries is large enough to prohibit a reliable extraction of G_E^n ⁵⁸.

This problem can be overcome, if the occurrence of e-n scattering is explicitly tagged through the detection of the outgoing neutron in coincidence with the scattered electron. Such an exclusive ${}^3\text{He}(\vec{e}, e'n)$ experiment was performed for the first time by the A3-collaboration at MAMI⁵⁷ at a squared four-momentum transfer of $Q^2 = 0.31 (\text{GeV}/c)^2$. With the detector-setup described in the following section the statistics was improved later on⁵⁹. The most recent experiment at $Q^2 = 0.67 (\text{GeV}/c)^2$ used the 3-spectrometer setup⁶⁰ of the A1-collaboration at MAMI^{61,62}.

In this experiment the target gas was polarized by metastable optical pumping and subsequently compressed to 6 bars. The relaxation time of approximately one day required twice a day the replacement of the target cell by a freshly polarized one. Quasi-elastic measurements were performed with target spin aligned perpendicular and parallel to the momentum transfer direction in order to access both the transverse asymmetry, A_x , and the longitudinal asymmetry, A_z . This enabled a measurement of the ratio A_x/A_z , which is directly proportional to G_E^n/G_M^n but independent of both the absolute degrees of beam and target polarization, P_e and P_T , respectively. Furthermore, the product $P_e \cdot P_T$ was monitored through the *elastic* measurement ${}^3\text{He}(e, e')$ in spectrometer B of the 3-spectrometer setup.

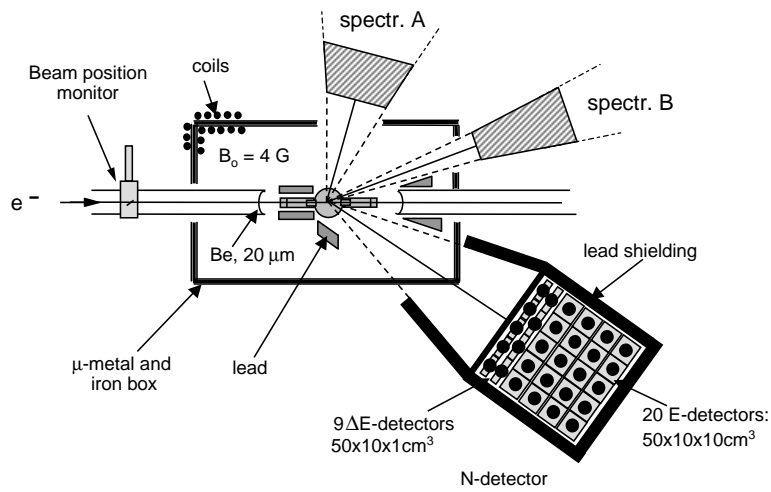


Figure 3. Target area of the ${}^3\text{He}(\vec{e}, e'n)$ experiment at MAMI. The cell with polarized gas is magnetically shielded against the spectrometers fringe fields.

The quasi-elastically scattered electrons were detected in spectrometer A (c.f. Fig.3), the neutrons in coincidence in a dedicated neutron detector provided by the University of Basel. It consisted of four layers of five plastic scintillators of dimensions $50 \times 10 \times 10 \text{ cm}^3$, which were equipped with photomultipliers at both ends. Charged particles could be rejected by means of two layers of 1 cm thick ΔE -counters. The neutron detector was shielded with 2 cm of lead against direct target sight in order to reduce the charged background.

The setup of the JLab Hall C $\vec{D}(\vec{e}, e'n)$ experiment in principle is similar ^{63,56}. Here the scattered electrons are detected in the HMS spectrometer in coincidence with neutrons in a segmented plastic scintillator. At the required luminosity of $1 \cdot 10^{35} \text{ cm}^{-2} \text{ s}^{-1}$ a 40% polarization of the ND_3 target is achieved by the technique of dynamic nuclear polarization. The deuteron nuclei are polarized by microwave irradiation at temperatures around 1 K in a strong magnetic field of 5 T. In the measurement of A_x this field deflects the incoming electron beam by as much as 4° . This has to be compensated by a magnetic chicane in order to guarantee horizontal beam at the center of the target. Data have been taken in the Q^2 range between 0.5 and $2 (\text{GeV}/c)^2$, first results are available at the lowest Q^2 ⁵⁶.

In contrast to MAMI and JLab, the NIKHEF $\vec{D}(\vec{e}, e'n)$ experiment was performed with a vector polarized *internal* gas target at the AmPS electron storage ring ⁵⁵. The scattered electrons were detected in coincidence simultaneously with protons and neutrons. Thus the asymmetry ratio between the $\vec{D}(\vec{e}, e'n)$ and $\vec{D}(\vec{e}, e'p)$ reactions could be determined.

3.2.2. The $D(\vec{e}, e'\vec{n})$ recoil polarization experiment at MAMI

As in the case of polarized targets a pioneering recoil polarization experiment was performed at MIT-Bates ⁶⁴. Electrons and neutrons from the $D(\vec{e}, e'\vec{n})$ reaction were detected in coincidence and the transverse neutron polarization, P_x , was measured. However, due to the low duty cycle of the Bates linac only modest statistical accuracy could be achieved. Furthermore, the external absolute calibration of the neutron polarimeter's effective analyzing power remained unsatisfactory.

The full potential of the recoil polarization method was exploited for the first time at MAMI. Fig.4 shows the experimental setup of this experiment. The longitudinally polarized electron beam ($I \simeq 2.5 \mu\text{A}$, $P_e \simeq 75\%$) impinged on a 5 cm long liquid deuterium target and the scattered electrons were detected in a 256 element lead glass array, which covered a solid

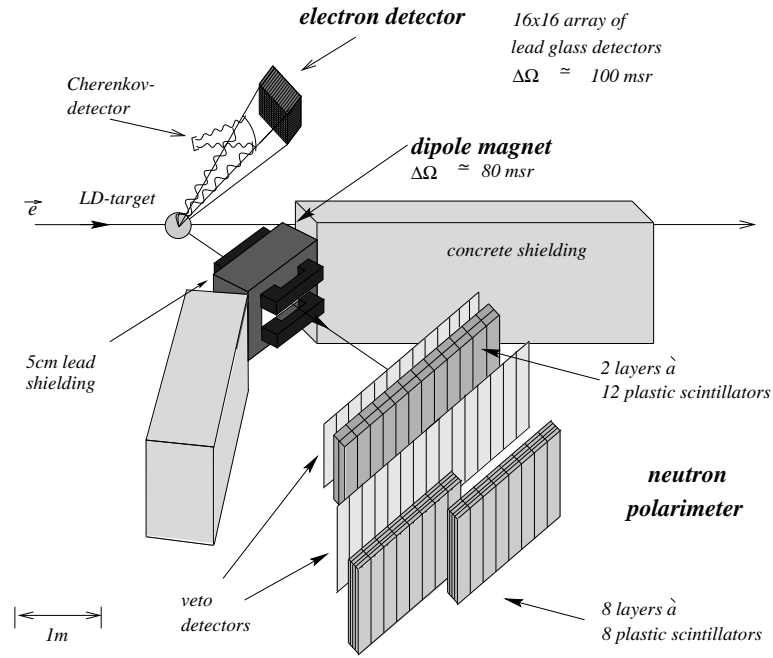
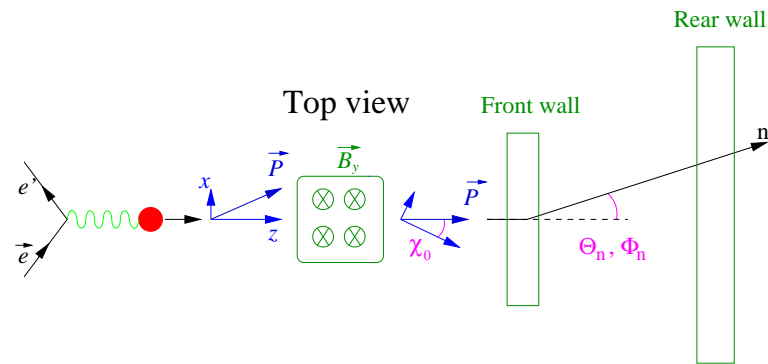
Figure 4. Setup of the $D(\vec{e}, e' \vec{n})$ experiment at MAMI

Figure 5. Schematics of the spin precession

angle of $\Delta\Omega \simeq 100$ msr. The energy resolution of $\delta E/E \simeq 25\%$ was sufficient to suppress pion production events. Only the electron angles, which were measured with an accuracy of approximately 3.5 mrad entered the

event reconstruction, which became kinematically complete through the measurement of the neutrons time-of-flight and hit position in the front plane of the neutron detector.

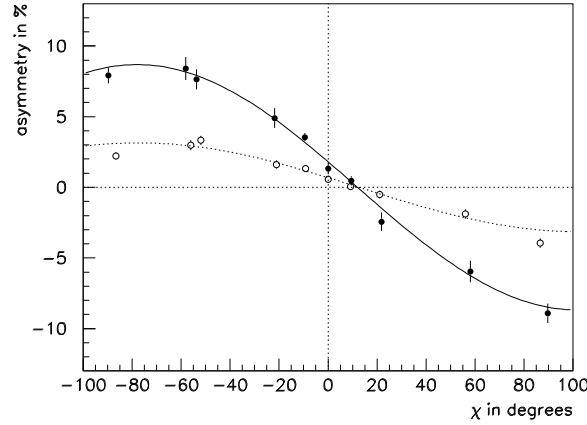


Figure 6. Transverse asymmetries as a function of the spin precession angle. The zero crossing is not affected by the different effective analyzing powers obtained by different conditions in the offline analysis (full and open points).

The neutron polarization can be analyzed in the detection process itself⁶⁵. This required a second neutron detection in one of the rear detector planes, which yielded the polar and azimuthal angles, Θ'_n and Φ'_n , of the analyzing scattering in the front wall. With the number of events $N^\pm(\Phi'_n)$ for \pm helicity states of the electron beam the azimuthal asymmetry, $A(\Phi'_n)$, was determined through the ratio

$$\frac{1 - A(\Phi'_n)}{1 + A(\Phi'_n)} = \sqrt{\frac{N^+(\Phi'_n) \cdot N^-(\Phi'_n + \pi)}{N^-(\Phi'_n) \cdot N^+(\Phi'_n + \pi)}}, \quad (19)$$

which is insensitive to variations of detector efficiency and luminosity. The extraction of P_x from $A(\Phi'_n) = \epsilon_{\text{eff}} \cdot P_x \cdot \sin \Phi'_n$ requires the calibration of the effective analyzing power, ϵ_{eff} , of the polarimeter. This, however, varies strongly with the event composition as determined by hardware conditions during data taking and software cuts applied in the offline analysis.

The problem of calibration of the effective analyzing power has been avoided by controlled precession of the neutron spins in the field of a dipole magnet in front of the polarimeter⁶⁶. This is schematically depicted in Fig. 5. After precession by the angle χ the transverse neutron polarization behind the magnet, P_\perp , is a superposition of x and z components, and likewise is the measured asymmetry:

$$A_\perp = A_x \cos \chi - A_z \sin \chi. \quad (20)$$

In the particular case of the zero crossing, $A_\perp(\chi_0) = 0$, one immediately gets the relation

$$\tan \chi_0 = \frac{A_x}{A_z} = \frac{\epsilon_{\text{eff}} \cdot P_e \cdot \sqrt{2\tau\epsilon(1-\epsilon)} G_E^n \cdot G_M^n}{\epsilon_{\text{eff}} \cdot P_e \cdot \tau \sqrt{1-\epsilon^2} (G_M^n)^2}. \quad (21)$$

Obviously, this ratio is independent of both the degree of electron beam polarization, P_e , and the polarimeter's effective analyzing power. It therefore directly yields G_E^n/G_M^n . Different effective analyzing powers do change the magnitude of the transverse asymmetry, A_\perp , but not the zero crossing angle, χ_0 ⁶⁶. This is demonstrated in Fig. 6, where A_\perp is plotted for two different cut conditions in the offline analysis (full and open points) as a function of the spin precession angle, χ . The magnitude of the asymmetry is affected but the zero crossing remains unchanged.

Using the established method of neutron spin precession a very similar experiment of the A1 collaboration at MAMI covers the extended Q^2 range up to $0.8 (\text{GeV}/c)^2$ ^{67,68,69}. Given the maximum beam energy of 880 MeV this requires neutron detection at forward angles of $\Theta_n^{\text{lab}} \simeq 27^\circ$ in a highly segmented neutron polarimeter.

3.3. Results

Even for quasi-free $D(e, e'n)$ scattering FSI effects are substantial below $Q^2 \simeq 0.3 (\text{GeV})^2$ and have been taken into account in the recent analyses using the calculations of Arenhövel⁵⁰. They drop rapidly with increasing Q^2 , increasing G_E^n for the MAMI/A3 data sample by almost a factor of two at $Q^2 = 0.12 (\text{GeV})^2$ but only $\simeq 10\%$ at $0.32 (\text{GeV})^2$ ⁷¹. Despite its size, the required correction of the G_E^n/G_M^n ratio has only small uncertainties, because it is insensitive to the choice of N-N potential and G_E^n parameterization^{50,70}. Therefore, even at $Q^2 = 0.12 (\text{GeV}/c)^2$ a reliable extraction of G_E^n/G_M^n is possible. This has been done relying on the dipole values for G_M^n (Eq.17).

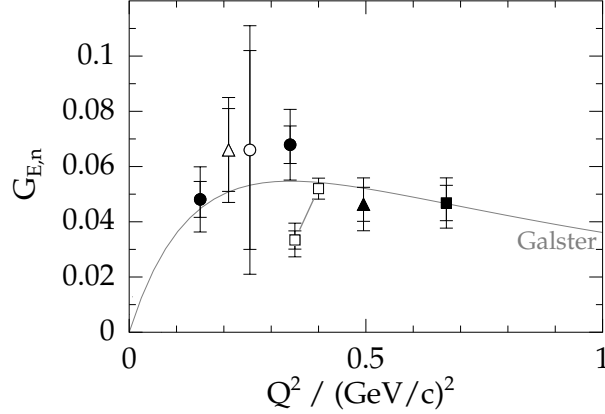


Figure 7. Results for $G_{E,n}^n$ from the $D(\vec{e}, e' \vec{n})$ experiment at MAMI (full circles)^{66,71} along with the ${}^3\text{He}(\vec{e}, e' n)$ results from MAMI (full square^{61,62}, open squares⁵⁹ with and without FSI correction), the $D(\vec{e}, e' \vec{n})$ result from Bates (open circle)⁶⁴, and the $\vec{D}(\vec{e}, e' n)$ results from NIKHEF (open triangle⁵⁵) and JLab (full triangle⁵⁶). Except the Bates data point the deuterium results are FSI-corrected. The curve is the one-parameter Galster parameterization.⁴⁵

Fig. 7 gives a summary of the recent double polarization measurements with statistical (inner) and systematical (outer) errors. The recoil polarization experiments are depicted by circles, full for the MAMI results^{66,71} and open for the Bates one⁶⁴. The triangles indicate the NIKHEF⁵⁵ and JLab⁵⁶ measurements with polarized deuteron target. The squares represent the MAMI results for ${}^3\text{He}(\vec{e}, e' n)$ ^{59,61,62}. For the ${}^3\text{He}$ experiments FSI is expected to be small at $Q^2 = 0.67 (\text{GeV}/c)^2$ ^{61,62}, due to the large kinetic energy of the ejected neutron. Contrary, at $Q^2 = 0.36 (\text{GeV}/c)^2$ (open squares)⁵⁹ first, still incomplete, Faddeev calculations indicate a substantial correction of the ${}^3\text{He}(\vec{e}, e' n)$ data point towards larger $G_{E,n}^n$. At the present status of calculation where no meson exchange currents are yet included the central value of the extracted $G_{E,n}^n$ is shifted by approximately 50 %³⁵. Due to the kinematical reconstruction the average Q^2 is also affected. Despite the small statistical error, this data point is subject to the largest systematical and theoretical (model) uncertainty, which is not included in the depicted error.

All polarization data lie above the so far favoured result from elastic $D(e, e')$ scattering, where the Paris potential has been used for the unfolding of the wave function contribution⁴⁶. They are compatible with the older

Galster parameterization⁴⁵

$$G_E^n = -\frac{\mu_n \tau}{1 + \eta \tau} \cdot G_D \quad (22)$$

with $\eta = 5.6$, which is indicated by the line in Fig. 7.

4. Summary and Outlook

Elastic form factors are related to the distribution of charge and current and thus fundamental quantities characterizing the nucleon ground state. In the context of this conference they are a prerequisite for the extraction of strangeness-specific information from parity violating elastic electron scattering.

From single arm $e - p$ scattering precise proton magnetic form factor data are available up to $Q^2 = 30 (\text{GeV}/c)^2$, roughly exhibiting dipole behaviour. Electric and magnetic contributions have been separated using the Rosenbluth technique; the results are in agreement with $p(\vec{e}, e' \vec{p})$ measurements at low Q^2 . Above $Q^2 \simeq 1.5 (\text{GeV}/c)^2$ the double polarization experiments have shown the ratio $\mu_p G_E^p / G_M^p$ to linearly fall below unity, G_E^p remaining only about 30 % of the dipole value at $Q^2 = 5.6 (\text{GeV}/c)^2$.

The neutron magnetic form factor, G_M^n , could be extracted up to $Q^2 = 4 (\text{GeV}/c)^2$ from single arm $D(e, e')$ quasi-elastic scattering. Below $Q^2 = 1 (\text{GeV}/c)^2$, recent coincidence experiments allowed a precise determination of G_M^n from the ratio $R = \frac{\sigma(e, e' n)}{\sigma(e, e' p)}$ of quasi-free electron scattering cross sections off the deuteron. Despite their individual statistical errors of only 2 %, two datasets from ELSA and MAMI/NIKHEF differ by as much as 10 - 15 %. This discrepancy contributed a substantial error to the extraction of strange form factors from parity violation. Recent independent results from $^3\text{He}(\vec{e}, e' n)$ measurements at $Q^2 \leq 0.6 (\text{GeV}/c)^2$ agree with the MAMI/NIKHEF dataset, however partially still relying on a simplified PWIA analysis. The full solution of this problem is also important with regard to the normalization of the recent double polarization experiments $^3\text{He}(\vec{e}, e' n)$, $\vec{D}(\vec{e}, e' n)$ and $D(\vec{e}, e' \vec{n})$ at various laboratories, where the neutron electric form factor is extracted from the ratio G_E^n / G_M^n of electric to magnetic neutron form factors.

In the $D(\vec{e}, e' \vec{n})$ experiment at MAMI the neutron polarimeter was supplemented by a spin precessing dipole magnet. This technique, which is also adopted for the corresponding JLab experiment, avoids the polarimeters analyzing power calibration. The influence of final state interaction has been quantitatively evaluated for the $D(\vec{e}, e' \vec{n})$ reaction. All recent double

polarization experiments are compatible with the old Galster parameterization.

It will be important to continue these G_E^n experiments at larger Q^2 . At JLab and MAMI there are further measurements underway, both with polarized target^{63,72} and recoil polarimetry^{73,67}. These experiments will further exploit the potential of double polarized quasi-elastic electron scattering.

5. Acknowledgements

The MAMI experiments have been performed within the framework of the collaborations A1 and A3 with contributions of institutes of the Universities of Basel, Bonn, Glasgow, Mainz, and Tübingen. H. Arenhövel supplied all the necessary calculations for the FSI correction of the deuteron measurements. The spin precession magnet for the $D(\vec{e}, e'\vec{n})$ experiment was provided by the Physikalisches Institut of the University of Bonn. The MAMI experiments are financially supported by the Deutsche Forschungsgemeinschaft (SFB 443).

References

1. T.E.O. Ericson and J. Hüfner, *Nucl. Phys.* **B 57** (1973) 604
2. S. Capstick and W. Roberts, *Prog. Part. Nucl. Phys.* **45**, 241 (2000) (nucl-th/0008028)
3. E.J. Hackett-Jones, D.B. Leinweber, and A.W. Thomas, *Phys. Lett. B* **494**, 89 (2000)
4. U. Wiese, priv. comm. (2003)
5. S.J. Dong et al., *Phys. Rev. D* **58**, 074504 (1997) and references therein
6. For a recent review see e.g. K. Goeke, M.V. Polyakov and M. Vanderhaeghen, *Prog. Part. Nucl. Phys.* **47**, 401 (2001)
7. A.V. Radyushkin, *Phys. Lett. B* **380**, 417 (1996)
8. X. Ji, *Phys. Rev. Lett.* **78**, 610 (1997) and *Phys. Rev. D* **55**, 7114 (1997)
9. T.A. Armstrong et al., *Phys. Rev. Lett.* **70**, 1212 (1993), and G. Bardin et al., *Nucl. Phys. B* **411**, 3 (1994) and references therein
10. A. Antonelli et al., *Nucl. Phys. B* **517**, 3 (1998)
11. J.D. Björken and S.D. Drell, *Relativistic quantum mechanics*, McGraw-Hill 1964
12. R.G. Sachs, *Phys. Rev.* **126**, 2256 (1962)
13. N. Isgur, *Phys. Rev. Lett.* **83**, 272 (1999)
14. F. Cardarelli and S. Simula, *Phys. Lett. B* **467**, 1 (1999)
15. D.B. Leinweber, A.W. Thomas, and R.D. Young, *Phys. Rev. Lett.* **86**, 5011 (2001)
16. M. Bawin and S.A. Coon, *Nucl. Phys. A* **689**, 475 (2001)

17. P. Bosted et al., *Phys. Rev. Lett.* **68**, 3841 (1992)
18. A.F. Sill et al., *Phys. Rev. D* **48**, 29 (1993)
19. R.G. Arnold et al., *Phys. Rev. Lett.* **57**, 174 (1986)
20. A.I. Akhiezer and M.P. Rekalo, *Sov. J. Part. Nucl.* **3**, 277 (1974)
21. R.G. Arnold et al., *Phys. Rev. C* **23**, 363 (1981)
22. M.K. Jones et al., AIP Conference Proceedings **412** (1997) 342
23. M.K. Jones et al., *Phys. Rev. Lett.* **84**, 1398 (2000)
24. O. Gayou et al., *Phys. Rev. C* **64**, 038202 (2001)
25. O. Gayou et al., *Phys. Rev. Lett.* **88**, 092301 (2002)
26. E.J. Brash, *Phys. Rev. C* **65**, 051001 (2002)
27. B. Milbrath et al., *Phys. Rev. Lett.* **80**, 452 (1998), erratum *Phys. Rev. Lett.* **82**, 2221 (1999)
28. Th. Pospischil et al., *Eur. Phys. J. A* **12**, 125 (2001)
29. Ch. Berger et al., *Phys. Lett. B* **35**, 87 (1971)
30. W. Bartel et al., *Nucl. Phys. B* **58**, 429 (1973)
31. L. Andivahis et al., *Phys. Rev. D* **50**, 5491 (1994)
32. R.C. Walker et al., *Phys. Rev. D* **49**, 5671 (1994)
33. for a compilation see I. Sick, Proc. 6th Miniconference on electron scattering, p. 193, NIKHEF 1989
34. A. Lung et al., *Phys. Rev. Lett.* **70**, 718 (1993)
35. J. Golak et al., *Phys. Rev. C* **63**, 034006 (2001)
36. H. Gao et al., *Phys. Rev. C* **50**, R546 (1994)
37. H. Gao, Bates25, Cambridge, MA, AIP Conference Proceedings **520** (1999)
38. W. Xu et al., *Phys. Rev. Lett.* **85**, 2900 (2000)
39. W. Xu et al., *Phys. Rev. C* **67**, 012201 (2003)
40. P. Markowitz et al., *Phys. Rev. C* **48**, R5 (1993)
41. H. Anklin et al., *Phys. Lett. B* **336**, 313 (1994)
42. E. Bruins et al., *Phys. Rev. Lett.* **75**, 21 (1995)
43. H. Anklin et al., *Phys. Lett. B* **428**, 248 (1998)
44. G. Kubon et al., *Phys. Lett. B* **524**, 26 (2002), nucl-ex/0107016
45. S. Galster et al., *Nucl. Phys. B* **32**, 221 (1971)
46. S. Platchkov et al., *Nucl. Phys. A* **510**, 740 (1990)
47. R. Schiavilla and I. Sick, *Phys. Rev. C* **64**, 041002(R) (2001)
48. J. Jourdan et al., *Phys. Rev. Lett.* **79**, 5186 (1997)
49. E. Bruins et al., *Phys. Rev. Lett.* **79**, 5187 (1997)
50. H. Arenhövel, *Phys. Lett. B* **199**, 13 (1987) and *Z. Phys. A* **331**, 509 (1988)
51. G. Eckert et al., *Nucl. Instr. Meth. A* **320**, 53 (1992) and W. Heil et al., *Phys. Lett. A* **201**, 337 (1995)
52. C.E. Woodward et al., *Phys. Rev. Lett.* **65**, 698 (1990)
53. T.E. Chupp et al., *Phys. Rev. C* **45**, 915 (1992)
54. J. Friar, *Phys. Rev. C* **42**, 2310 (1990)
55. I. Passchier et al., *Phys. Rev. Lett.* **82**, 4988 (1999)
56. H. Zhu et al., *Phys. Rev. Lett.* **87**, 081801 (2001)
57. M. Meyerhoff et al., *Phys. Lett. B* **327**, 201 (1994)
58. R. Schulze and P. Sauer, *Phys. Rev. C* **48**, 38 (1993)
59. J. Becker et al., *Eur. Phys. J. A* **6**, 329 (1999)

60. K.I. Blomqvist et al., *Nucl. Instr. Meth. A* **403**, 263 (1998)
61. D. Rohe et al., *Phys. Rev. Lett.* **83**, 4257 (1999)
62. J. Bermuth, AIP conference proceedings **603**, 331 (2001)
63. D. Day et al., JLab proposal E-93-026 (1993)
64. T. Eden et al., *Phys. Rev. C* **50**, R1749 (1994)
65. T.N. Taddeucci et al., *Nucl. Instr. Meth. A* **241**, 448 (1985)
66. M. Ostrick et al., *Phys. Rev. Lett.* **83**, 276 (1999)
67. U. Müller and H. Schmieden et al., MAMI proposal A1/2-99 (1999)
68. M. Seimetz, doctoral thesis, Mainz (in preparation)
69. D. Glazier, doctoral thesis, Glasgow (in preparation)
70. H. Arenhövel, priv. comm., 1998
71. C. Herberg et al., *Eur. Phys. J. A* **5**, 131 (1999)
72. W. Heil et al., MAMI proposal A1/4-95 (1995)
73. R. Madey and S. Kowalski et al., JLab proposal E93-038 (1993)